

RESEARCH ARTICLE

# Reticulon and CLIMP-63 regulate nanodomain organization of peripheral ER tubules

Guang Gao, Chengjia Zhu , Emma Liu , Ivan R. Nabi \*

Department of Cellular and Physiological Sciences, Life Sciences Institute, University of British Columbia, Vancouver, Canada

 These authors contributed equally to this work.

\* [irnabi@mail.ubc.ca](mailto:irnabi@mail.ubc.ca)



 OPEN ACCESS

**Citation:** Gao G, Zhu C, Liu E, Nabi IR (2019) Reticulon and CLIMP-63 regulate nanodomain organization of peripheral ER tubules. *PLoS Biol* 17 (8): e3000355. <https://doi.org/10.1371/journal.pbio.3000355>

**Academic Editor:** Sandra L. Schmid, UT Southwestern Medical Center, UNITED STATES

**Received:** February 19, 2019

**Accepted:** July 26, 2019

**Published:** August 30, 2019

**Copyright:** © 2019 Gao et al. This is an open access article distributed under the terms of the [Creative Commons Attribution License](https://creativecommons.org/licenses/by/4.0/), which permits unrestricted use, distribution, and reproduction in any medium, provided the original author and source are credited.

**Data Availability Statement:** All relevant data are within the paper and its Supporting Information files.

**Funding:** This work was supported by the Canadian Institutes of Health Research (PJT-148698), the National Science and Engineering Research Council of Canada (RGPIN 227925-13), and the Canada Foundation for Innovation/British Columbia Knowledge Development Fund (LEF 30636) to IRN. GG is the recipient of a UBC Four Year Doctoral Fellowship and CZ the recipient of an NSERC Undergraduate Student Research Award.

## Abstract

The endoplasmic reticulum (ER) is an expansive, membrane-enclosed organelle composed of smooth peripheral tubules and rough, ribosome-studded central ER sheets whose morphology is determined, in part, by the ER-shaping proteins, reticulon (RTN) and cytoskeleton-linking membrane protein 63 (CLIMP-63), respectively. Here, stimulated emission depletion (STED) super-resolution microscopy shows that reticulon4a (RTN4a) and CLIMP-63 also regulate the organization and dynamics of peripheral ER tubule nanodomains. STED imaging shows that luminal ER monomeric oxidizing environment-optimized green fluorescent protein (ERmoxGFP), membrane Sec61βGFP, knock-in calreticulin-GFP, and antibody-labeled ER-resident proteins calnexin and derlin-1 are all localized to periodic puncta along the length of peripheral ER tubules that are not readily observable by diffraction limited confocal microscopy. RTN4a segregates away from and restricts luminal blob length, while CLIMP-63 associates with and increases luminal blob length. RTN4a and CLIMP-63 also regulate the nanodomain distribution of ER-resident proteins, being required for the preferential segregation of calnexin and derlin-1 puncta away from luminal ERmoxGFP blobs. High-speed (40 ms/frame) live cell STED imaging shows that RTN4a and CLIMP-63 regulate dynamic nanoscale luminal compartmentalization along peripheral ER tubules. RTN4a enhances and CLIMP-63 disrupts the local accumulation of luminal ERmoxGFP at spatially defined sites along ER tubules. The ER-shaping proteins RTN and CLIMP-63 therefore regulate luminal ER nanodomain heterogeneity, interaction with ER-resident proteins, and dynamics in peripheral ER tubules.

## Introduction

Since the initial Singer-Nicholson fluid mosaic model of free membrane diffusion in the 1980s, the role of membrane nanodomains in the control of protein and lipid dynamics in the plasma membrane, regulating signal transduction, endocytosis and exocytosis, and thereby cellular behavior has been extensively characterized [1]. In contrast, the nanodomain organization of organellar membrane structures remains poorly defined.

The endoplasmic reticulum (ER) is a continuous membrane network that is classically divided into central ribosome-studded rough ER sheets, the site of protein synthesis, and

The funders had no role in study design, data collection and analysis, decision to publish, or preparation of the manuscript.

**Competing interests:** The authors have declared that no competing interests exist.

**Abbreviations:** ATL, atlastin; BiP, binding immunoglobulin protein; CLIMP-63, cytoskeleton-linking membrane protein 63; CoV, coefficient of variation; Cas9, CRISPR-associated protein 9; CRISPR, clustered regularly interspaced palindromic repeat; CTL, control; DP1, deleted in polyposis 1; ER, endoplasmic reticulum; ERAD, ER-associated protein degradation; ERmoxGFP, ER monomeric oxidizing environment-optimized green fluorescent protein; FBS, fetal bovine serum; FWHM, full width at half maximum; GI-SIM, grazing incidence structured illumination microscopy; Gp78, glycoprotein 78; GRP78, glucose-regulated protein 78; KDEL, Lys-Asp-Glu-Leu; KI, knock-in; mRFP, monomeric red fluorescent protein; PBS, Phosphate-Buffered Saline; ROI, region of interest; RTN, reticulon; RTN4a, reticulon4a; SD, standard deviation; siRNA, small interfering RNA; STED, stimulated emission depletion; Stx17, Syntaxin-17; 2D, two-dimensional; 3D, three-dimensional.

peripheral smooth ER tubules, implicated in lipid synthesis and detoxification [2–5]. A family of ER-shaping proteins that maintain sheet or tubule architecture include the cytoskeleton-linking membrane protein 63 (CLIMP-63), ribosome-interacting protein p180, reticulon (RTN), atlastin (ATL), and deleted in polyposis 1 (DP1/Yop1p) [4–8]. RTN has two hydrophobic hairpins that could form a wedge-like structure, causing local ER curvature by replacing the lipids in the outer leaflet of the lipid bilayer [9], and has been implicated in peripheral ER tubule formation [3,10–12]. CLIMP-63 is predominantly associated with central ER sheet formation and has been proposed to function as a spacer that maintains ER sheets [6]. ATL induces membrane fusion and the formation of three-way junctions [4,8]. RTN family member reticulon4a (RTN4a) induces the expansion of peripheral ER tubules, while CLIMP-63 promotes ER sheet formation; the relative expression of these two ER-shaping proteins determines the cellular abundance of ER sheets versus tubules [3,6,12]. CLIMP-63 has also been localized to peripheral ER tubules [13] and, here, we use stimulated emission depletion (STED) super-resolution imaging to show that RTN4a and CLIMP-63 regulate the nanodomain organization and dynamics of peripheral ER tubules.

The thickness of an ER sheet and the diameter of an ER tubule are typically 30–100 nm [2,14], below the diffraction limit of visible light (approximately 200 nm), hindering the characterization of ER structure by standard confocal fluorescence microscopy. In addition to these spatial limitations, the ER is a highly dynamic organelle and its study in live cells requires high temporal resolution; recent use of high-speed, super-resolution imaging techniques suggested that peripheral ER sheets are densely packed tubular arrays [13]. STED super-resolution microscopy [15] obtains lateral resolution of approximately 50 nm, and the pioneering application of STED imaging to the ER revealed ring structures formed by the tubular network of the ER that were not observed by conventional confocal microscopy [16]. A more recent STED analysis identified the presence of dynamic nanoholes in peripheral ER sheets [17]. Single molecule super-resolution particle tracking of an ER luminal reporter demonstrated the existence of active ER luminal flow in peripheral ER tubules [18], while high-speed, super-resolution grazing incidence structured illumination microscopy (GI-SIM) identified luminal bulges and constrictions along ER tubules [19].

However, molecular mechanisms that regulate the organization of ER nanodomains remain to be defined. Here, we apply STED microscopy to study luminal compartmentalization in peripheral ER tubules using the luminal ER reporter ER monomeric oxidizing environment-optimized green fluorescent protein (ERmoxGFP). ERmoxGFP contains the bovine prolactin signal sequence and Lys-Asp-Glu-Leu (KDEL) ER retention sequence linked to monomeric, cysteine-less moxGFP, a modified inert GFP optimized for use in oxidizing environments that minimally perturbs the cell [20]. We find that ERmoxGFP defines local luminal filling of nanodomains that are segregated from membrane-associated ER proteins along peripheral ER tubules. RTN enhances and CLIMP-63 disrupts the spatial localization of these luminal nanodomains along ER tubules, thereby impacting the segregation of membrane-associated ER proteins from luminal ER nanodomains.

## Results

### STED super-resolution microscopy reveals nanoscale periodicity in ER tubules

The peripheral ER imaged by diffraction limited confocal microscopy presents a highly reticular network of interconnected ER tubules. Super-resolution two-dimensional (2D) STED live cell imaging of HT-1080 fibrosarcoma and COS-7 cells transfected with the ER luminal reporter ERmoxGFP [20] shows that peripheral ER tubules are highly periodic and composed

of tubules showing discrete densities of ERmoxGFP (Fig 1A). Peripheral ER tubule periodicities are observed by 2D STED live cell imaging of ERmoxGFP transfected HT-1080 and COS-7 cells, at a temporal resolution of 0.8 seconds per frame (S1 Video). Peripheral ER tubule periodicities are also observed in cells fixed with 3% paraformaldehyde/0.2% glutaraldehyde (Fig 1A), an established fixation protocol that preserves ER architecture [13,21–23].

Line scan analysis shows distinct maxima and minima corresponding to local enrichment and depletion, respectively, of the fluorescent signal from the luminal ERmoxGFP reporter along peripheral ER tubules in fixed and live cells (Fig 1B). ER tubule line scan analysis of raw STED images matches that of the deconvolved image; deconvolution effectively reduces noise along the line scan, which is increased for live cell scans due to refractive index mismatching of the imaging media, without impacting blob (maxima) size or distribution (Fig 1B). ER luminal blob length, determined from the full width at half maximum (FWHM) measurement of maxima in line scan analysis, is equivalent along ER tubules in both live and fixed cells (Fig 1C). STED analysis of fixed cells has therefore retained nanodomain features of ER tubules observed in live cells.

As RTN4a promotes ER tubule formation [3,10–12], we therefore assessed whether it also regulates peripheral ER tubule periodicity. Upon RTN4 small interfering RNA (siRNA) knockdown, luminal ERmoxGFP-labeled maxima in peripheral ER tubules are elongated relative to control (Fig 2A and 2B), as indicated by arrowheads; CLIMP-63 siRNA knockdown did not alter the periodic distribution of this luminal ER reporter (Fig 2A and 2B). To quantify peripheral ER tubule periodicity, we measured maxima (blob) length, variation in maxima length (standard deviation [SD]) and maxima-to-minima fluorescence intensity differentials from line scans of ER tubules (i.e., Fig 1B). Significantly increased maxima length, increased variation of maxima length, and reduction in maxima-to-minima intensity differential are observed for ER tubules of RTN4 knockdown cells (Fig 2C). No significant changes in these parameters were observed for ER tubules of CLIMP-63 knockdown cells (Fig 2C) compared with cells transfected with control siRNA. This suggests that RTN4 not only induces peripheral ER tubule formation but also regulates the nanodomain organization of these ER tubules.

We then tested whether overexpression of mCherry-RTN4a, mCherry-CLIMP-63, and, as a control, mCherry-ATL1, impacts luminal nanodomain organization in peripheral ER tubules. ERmoxGFP-transfected HT-1080 cells show expansion of the central ER and reduction of peripheral tubules upon mCherry-CLIMP-63 overexpression, formation of an extended network of peripheral tubules upon mCherry-RTN4a overexpression, and increased branched peripheral ER structures upon mCherry-ATL1 overexpression (Fig 3A), consistent with previous reports on these ER-shaping proteins [3,6,9,12,24]. Similar to RTN4 knockdown (Fig 2B and 2C), mCherry-CLIMP-63 overexpression induces the formation of elongated luminal ERmoxGFP blobs along ER tubules that overlap with mCherry-CLIMP-63 (Fig 3A). In contrast, upon mCherry-RTN4a overexpression, both ERmoxGFP and mCherry-RTN4a show highly periodic distributions that present minimal overlap (Fig 3A).

Line scan quantification of ERmoxGFP in peripheral ER tubules of HT-1080 cells shows that mCherry-CLIMP-63 transfection decreases luminal periodicity. ERmoxGFP tubules present significantly increased maxima length, increased variation in maxima length, and decreased maxima-to-minima intensity differentials. In contrast, overexpressed mCherry-RTN4a enhances the periodicity of ERmoxGFP, reducing the variation of maxima length and increasing maxima-to-minima intensity differentials. mCherry-ATL1 overexpression does not impact maxima length, variation of maxima length, or maxima-to-minima differentials (Fig 3B). To quantify the extent of overlap of ERmoxGFP nanodomains with the different ER-shaping proteins, we counted the number of ER-shaping protein puncta localized to ERmoxGFP maxima or minima in line scans of individual peripheral ER tubules. mCherry-CLIMP-63 is

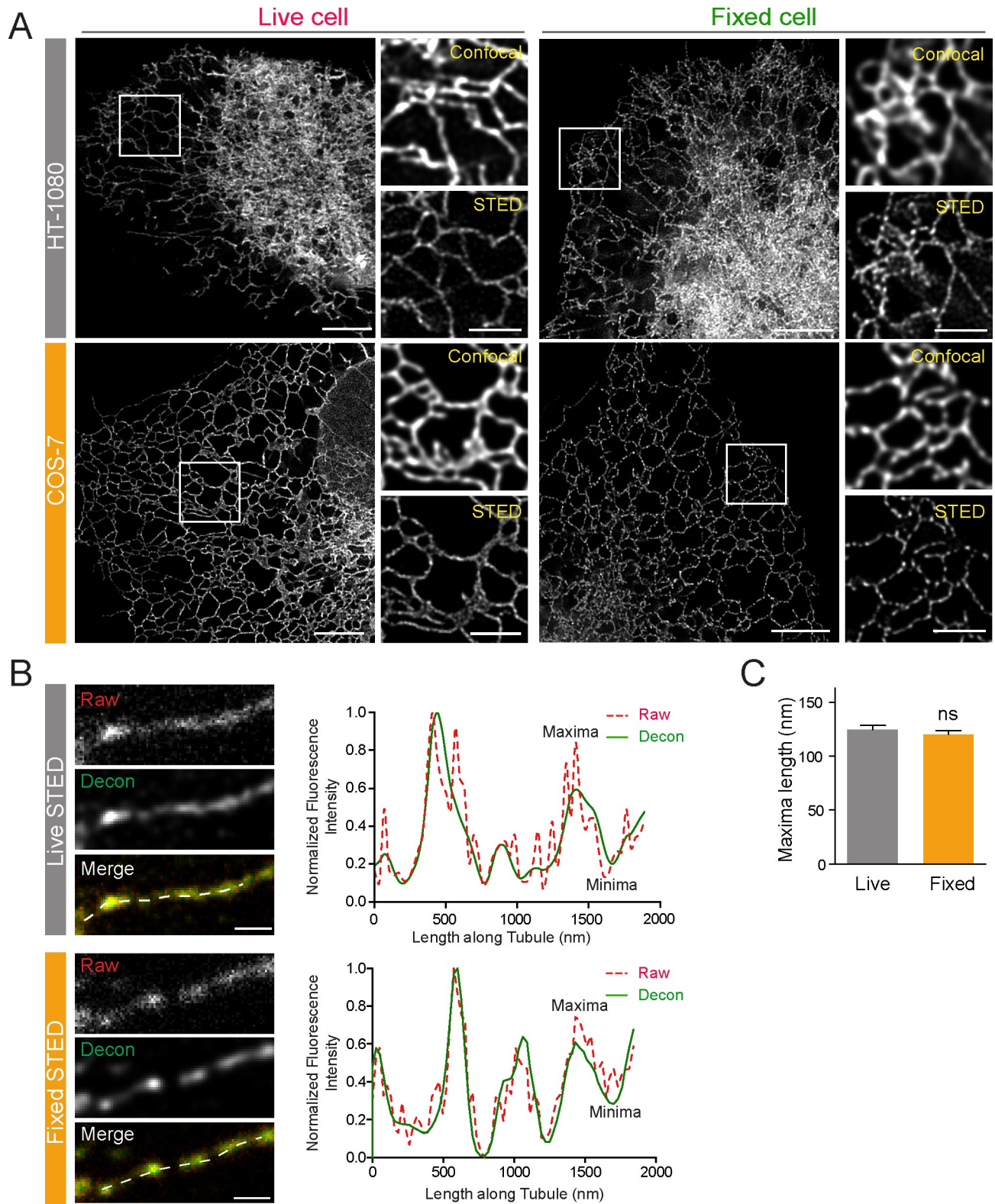


**Fig 1. STED imaging reveals luminal nanodomain periodicity in peripheral ER tubules.** (A) Representative 2D STED images of live and fixed HT-1080 or COS-7 cells expressing ERmoxGFP are shown. Magnified confocal and STED images of the boxed region highlight the improved resolution obtained by 2D STED. Scale bar, 5  $\mu$ m; zooms, 2  $\mu$ m. (B) Line scans of isolated peripheral ERmoxGFP-labeled tubules (dashed) from STED images of live and fixed cells show matching maxima and minima for raw (red, dashed) and deconvolved (decon, green, solid) images. Scale bar, 0.5  $\mu$ m. (C)

Length of ERmoxGFP maxima/blob was measured in 2D STED images of peripheral ER tubules in live and fixed cells. Values plotted are mean  $\pm$  SEM from three independent experiments (10–20 line scans/each repeat). Significance assessed by Student *t* test. Numerical values that underlie the graph are shown in [S1 Data](#). ER, endoplasmic reticulum; ERmoxGFP, ER monomeric oxidizing environment-optimized green fluorescent protein; ns, not significant; STED, stimulated emission depletion; 2D, two-dimensional.

<https://doi.org/10.1371/journal.pbio.3000355.g001>

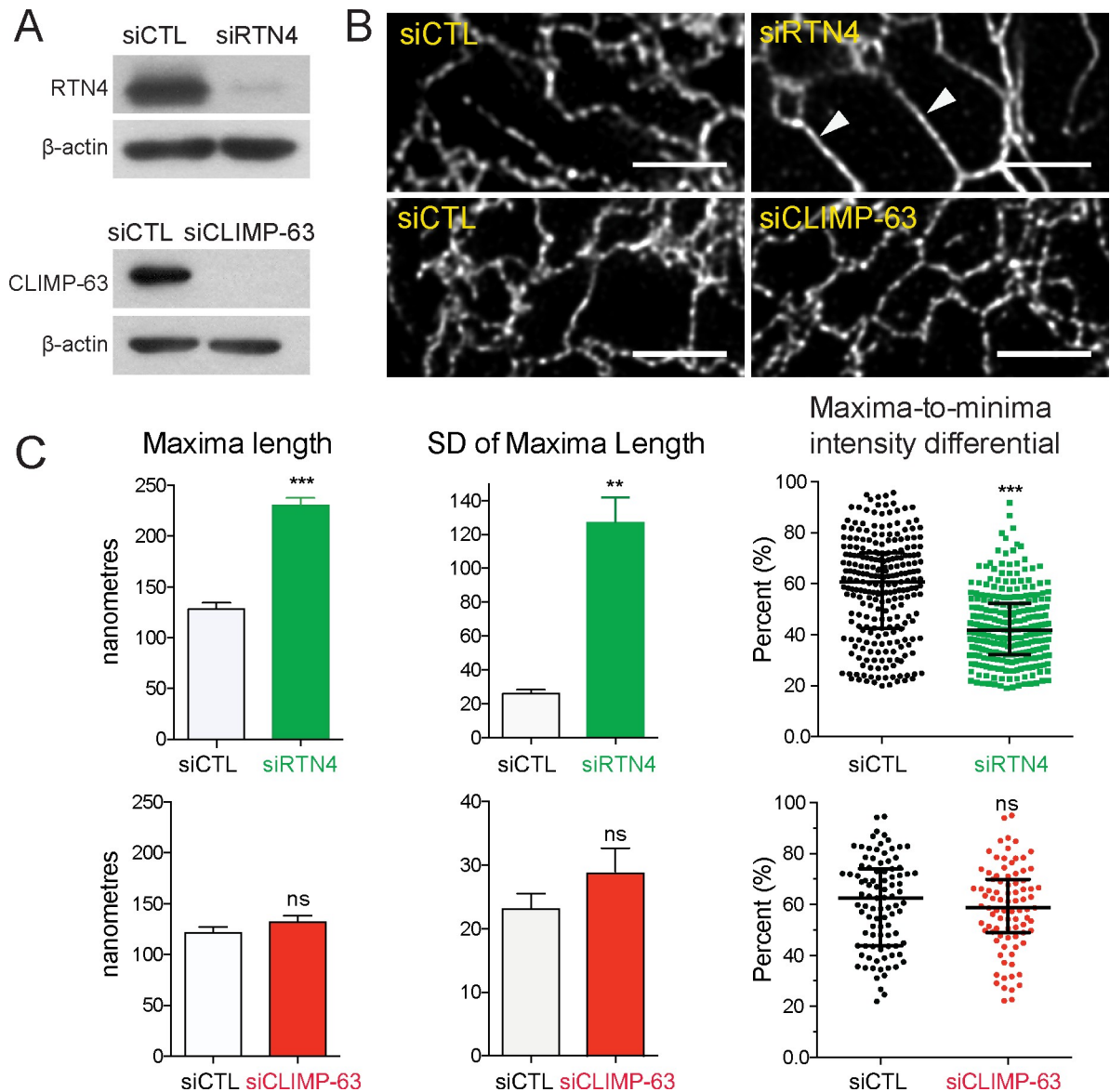


**Fig 2. RTN4 regulates luminal ER nanodomain periodicity.** (A) Western blots of siCTL-, siRTN4-, and siCLIMP-63-transfected HT-1080 cells were probed with anti-RTN4, anti-CLIMP-63, and anti- $\beta$ -actin as a loading control. (B) Representative images of ER tubules in HT-1080 cells transfected with ERmoxGFP and siCTL, siRTN4, or siCLIMP-63. Arrowheads indicate the tubules with increased blob length. Scale bar, 2  $\mu$ m. (C) The quantification of maxima length, variation of maxima length (SD), and maxima-minima intensity differentials of ER tubules in HT-1080 cells transfected with siRTN4, siCLIMP-63, or siCTL. Bar graphs show mean  $\pm$  SEM and scatter dot plots median with interquartile range. Significance assessed by Student *t* test from three independent experiments (20–40 line scans/each repeat). \*\*  $P < 0.01$ ; \*\*\*  $P < 0.001$ . Numerical values that underlie the graphs and plots are shown in [S1 Data](#). CLIMP-63, cytoskeleton-linking membrane protein 63; ER, endoplasmic reticulum; ERmoxGFP, ER monomeric oxidizing environment-optimized green fluorescent protein; ns, not significant; RTN4, reticulon4; SD, standard deviation; siCLIMP-63, siRNA to CLIMP-63; siCTL, siControl; siRTN4, siRNA to RTN4.

<https://doi.org/10.1371/journal.pbio.3000355.g002>

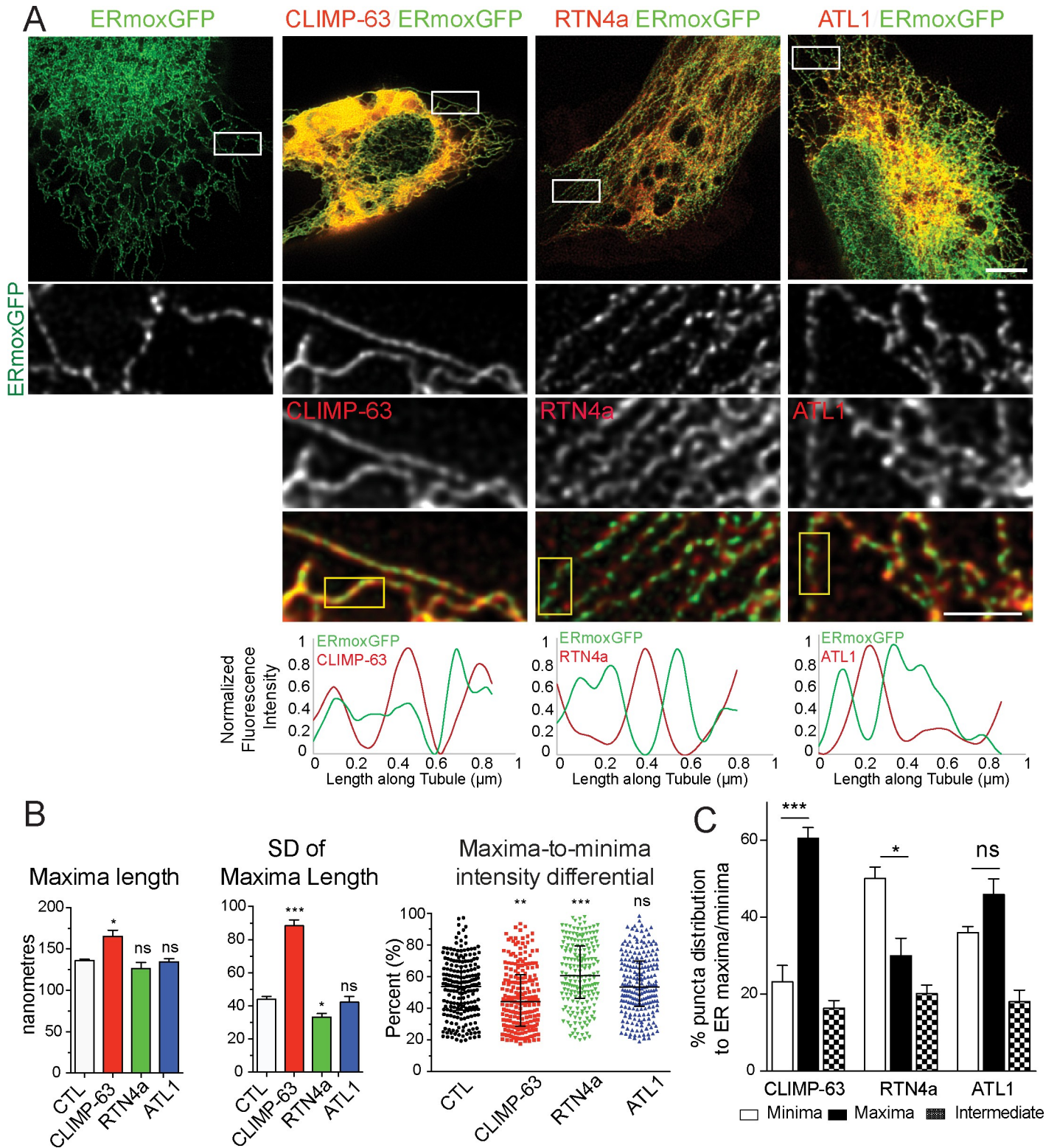


**Fig 3. RTN4a and CLIMP-63 overexpression differentially impacts ER nanodomain periodicity.** (A) STED images of ERmoxGFP in HT-1080 cells transfected with ERmoxGFP or cotransfected with mCherry-CLIMP-63 (CLIMP-63), mCherry-RTN4a (RTN4a), or mCherry-ATL1 (ATL1). Peripheral ER regions (white boxes) are shown as zooms; line scans of selected tubules in these regions (yellow boxes) are shown with ERmoxGFP in green and ER-shaping proteins in red. Scale bar, 5  $\mu\text{m}$ ; zooms, 2  $\mu\text{m}$ . (B) Peripheral ER tubule maxima length, variation of maxima length (SD), and maxima-to-minima intensity differential are shown for cells transfected with ERmoxGFP alone (CTL) or cotransfected with mCherry-CLIMP-63 (CLIMP-63), mCherry-RTN4a (RTN4a), or mCherry-ATL1 (ATL1). Significance assessed

by one-way ANOVA from three independent experiments (40 line scans/each repeat). Bar graphs show mean  $\pm$  SEM and scatter dot plots median with interquartile range. \* $P < 0.05$ ; \*\* $P < 0.01$ ; \*\*\* $P < 0.001$ . Numerical values that underlie the graphs and plots are shown in [S1 Data](#). (C) Based on line scan analysis of peripheral ER tubules of HT-1080 cells cotransfected with mCherry-CLIMP-63 (CLIMP-63), mCherry-RTN4a (RTN4a), or mCherry-ATL1 (ATL1), percent localization of CLIMP-63, RTN4a, and ATL1 puncta to minima or maxima of luminal ERmoxGFP-labeled tubules was quantified. Significance assessed by one-way ANOVA from four independent experiments (40 line scans/each repeat). Bar graphs show mean  $\pm$  SEM. \* $P < 0.05$ ; \*\*\* $P < 0.001$ . Numerical values that underlie the graphs are shown in [S1 Data](#). ATL, atlastin; CLIMP-63, cytoskeleton-linking membrane protein 63; CTL, control ER, endoplasmic reticulum; ERmoxGFP, ER monomeric oxidizing environment-optimized green fluorescent protein; ns, not significant; RTN4a, reticulon4a; SD, standard deviation; STED, stimulated emission depletion.

<https://doi.org/10.1371/journal.pbio.3000355.g003>

significantly associated with ERmoxGFP maxima, mCherry-RTN4a with minima, and mCherry-ATL1 shows no significant preference for maxima or minima ([Fig 3C](#)). This suggests that RTN4a is segregated away from, while CLIMP-63 is associated with, luminal ERmoxGFP-filled nanodomains.

### RTN4a and CLIMP-63 regulate nanodomain heterogeneity in peripheral ER tubules

We then undertook to determine whether other ER markers present a similar peripheral ER tubule periodicity. As observed for ERmoxGFP, the peripheral reticular network of Sec61 $\beta$ GFP-labeled tubules in live HT-1080 and COS-7 cells showed a highly periodic distribution by STED ([Fig 4A](#); [S1 Video](#)). Similarly, GFP-calreticulin expressed at endogenous levels by clustered regularly interspaced palindromic repeat (CRISPR)/CRISPR-associated protein 9 (Cas9) knock-in technology in U2OS cells [22] presents a tubular network by confocal and a highly periodic distribution by STED ([Fig 4A](#)) imaging. Two-dimensional STED imaging of fixed cells expressing ERmoxGFP and Sec61 $\beta$  tagged with monomeric red fluorescent protein (Sec61 $\beta$ -mRFP) show distinct patterns of nanodomain enrichment for these two ER reporters along ER tubules ([Fig 4B](#)).

We then extended our analysis to examine the distribution of the endogenous ER-resident proteins, calnexin and derlin-1, involved in protein quality control and ER-associated protein degradation (ERAD), respectively [25,26]. Antibody labeling of both calnexin and derlin-1 shows a reticular ER distribution by confocal microscopy in HT-1080 cells; by contrast, STED imaging of these endogenous ER proteins shows a highly punctate distribution ([Fig 4C](#)). A similar punctate distribution for calnexin is observed in both ERmoxGFP transfected and untransfected cells ([S1 Fig](#)), and is therefore not a result of overexpression of the luminal ERmoxGFP reporter. Two-dimensional STED images of fixed HT-1080 cells show that calnexin and derlin-1 puncta show minimal overlap and that many of these ER protein puncta align along ERmoxGFP-labeled tubules ([Fig 4D](#)). Three-dimensional (3D) STED analysis shows that the majority of calnexin and derlin-1 puncta are intercalated into the ERmoxGFP tubular network and that these two ER-resident proteins show minimal overlap ([Fig 4E](#); [S2 Video](#)), highlighting the nanodomain heterogeneity of peripheral ER tubules.

Quantitative line scan analysis of 2D STED imaged peripheral ER tubules shows the increased association of calnexin and derlin-1 puncta with ERmoxGFP minima and an equal distribution between minima and maxima of Sec61 $\beta$ GFP-labeled tubules ([Fig 5A and 5B](#)). Similarly, manual counting of the distribution of calnexin or derlin-1 puncta in peripheral 3D STED regions of interest (ROIs) ([Fig 4E](#)) shows the clear localization of protein puncta to minima between ERmoxGFP-labeled blobs (maxima) ([S2A Fig](#)). Line scan analysis of the distribution of three other ER proteins, binding immunoglobulin protein/glucose-regulated protein 78 (BiP/GRP78), glycoprotein 78 (Gp78), and Syntaxin-17 (Stx17), show a similar enriched distribution to ERmoxGFP minima along peripheral ER tubules ([S2B Fig](#)). This suggests that ER tubule nanodomains that present increased accumulation of the luminal ER reporter

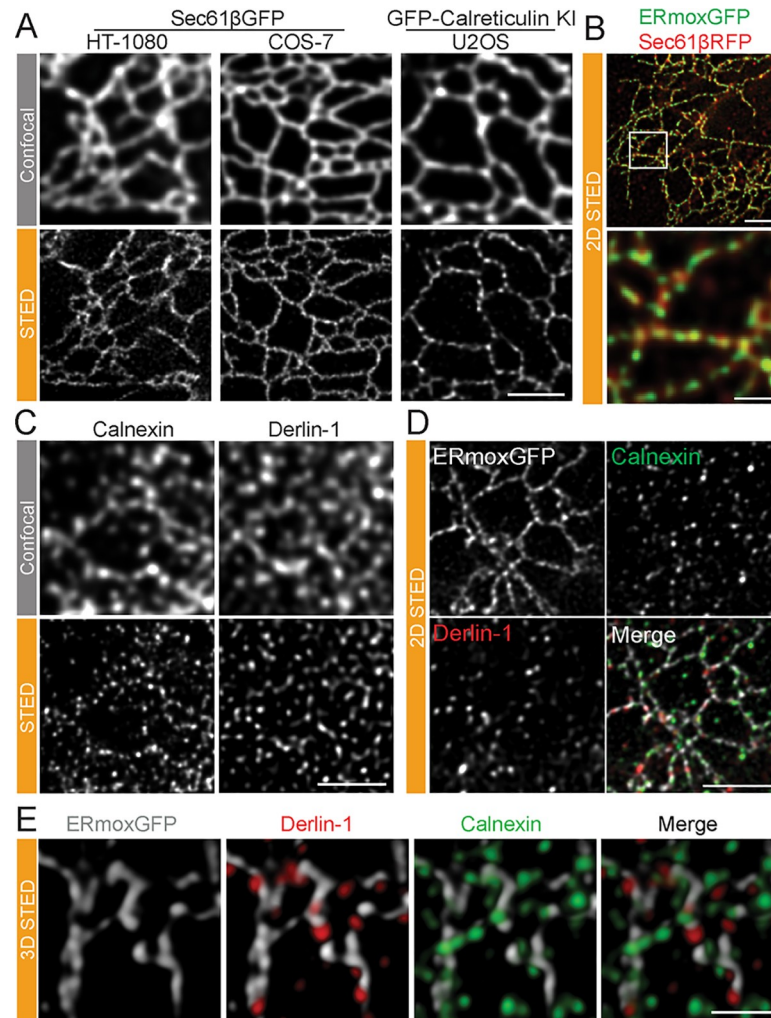


**Fig 4. Periodic distribution of other ER markers and ER-resident proteins along peripheral ER tubules.** (A) Representative confocal and STED images of live HT-1080 and COS-7 cells overexpressing Sec61βGFP or live knock-in U2OS cells expressing GFP-calreticulin at endogenous levels. Scale bar, 2 μm. (B) STED images of fixed HT-1080 cells expressing luminal ERmoxGFP (green) and membrane Sec61βmRFP (red) show distinct periodicity of these two ER reporters along peripheral ER tubules. Scale bar, 2 μm; zoom, 0.5 μm. (C) Untransfected HT-1080 cells labeled for derlin-1 or calnexin imaged by confocal and STED. Scale bar, 2 μm. (D) Association of ER-resident proteins derlin-1 and calnexin with ERmoxGFP-labeled peripheral ER tubules in HT-1080 cells by 2D STED. Scale bar, 2 μm. (E) Association of ER-resident proteins derlin-1 and calnexin with ERmoxGFP-labeled peripheral ER tubules in HT-1080 cells by 3D STED. Scale bar, 1 μm. ER, endoplasmic reticulum; ERmoxGFP, ER monomeric oxidizing environment-optimized green fluorescent protein; KI, knock-in; STED, stimulated emission depletion; 2D, two-dimensional; 3D, three-dimensional.

<https://doi.org/10.1371/journal.pbio.3000355.g004>

ERmoxGFP are segregated away from nanodomains enriched for ER-resident protein complexes.

We then tested if RTN4a and CLIMP-63 impact the distribution of ER-resident proteins to ER tubule nanodomains. Upon RTN4a or CLIMP-63 knockdown or RTN4a or CLIMP-63 overexpression, calnexin or derlin-1 puncta no longer showed a preferential distribution to minima of luminal ERmoxGFP but rather a balanced distribution to maxima and minima (Fig 5C and 5D). ATL1 overexpression did not significantly impact the distribution of ER protein puncta to luminal minima (Fig 5D). This suggests that RTN4a and CLIMP-63 regulate

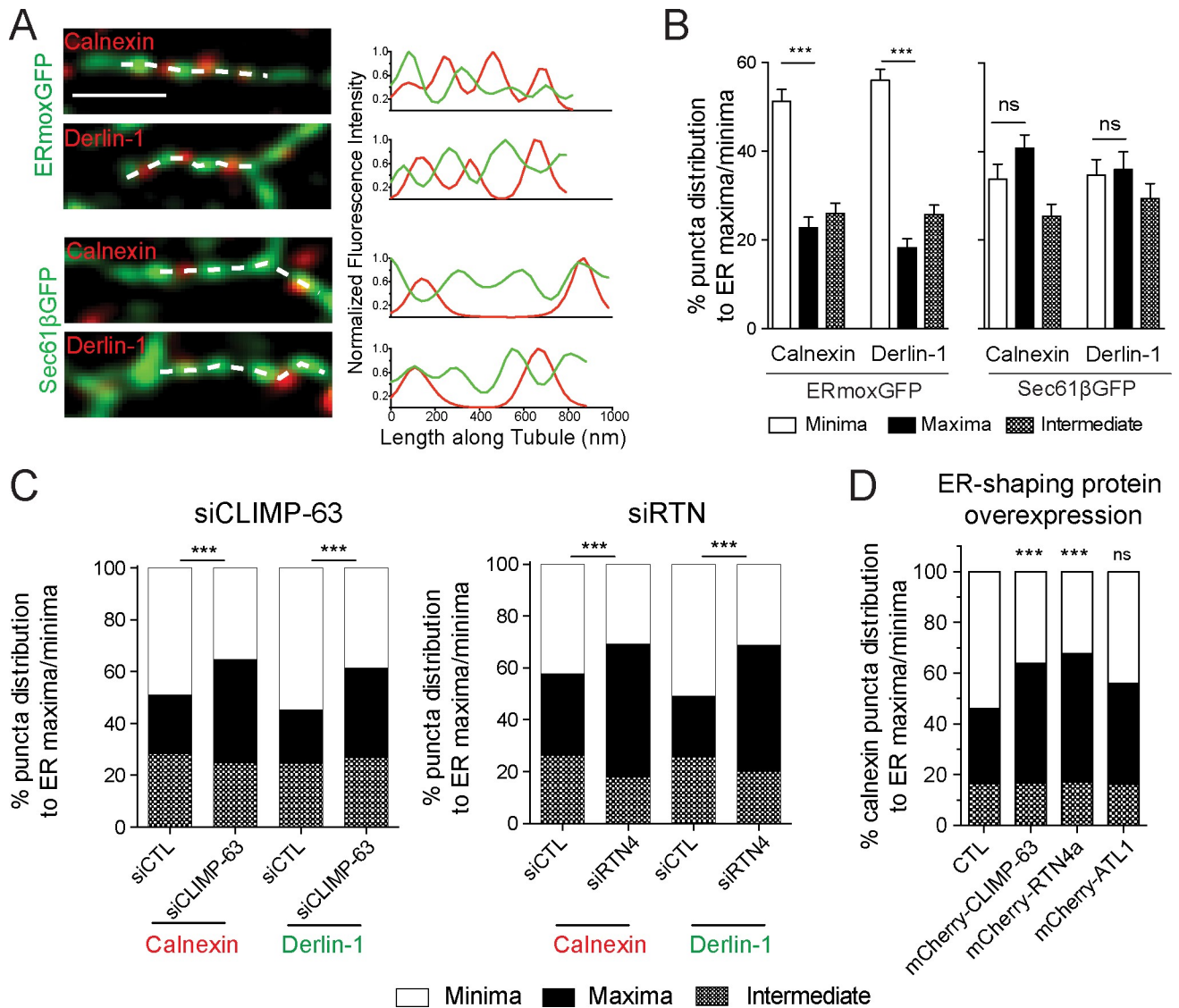


**Fig 5. ER-resident proteins calnexin and derlin-1 are enriched in nanodomains depleted of luminal ERmoxGFP.** (A) Representative merged images of single peripheral ER tubules expressing ERmoxGFP or Sec61βGFP labeled for calnexin or derlin-1. The dashed line indicates the site of line scan analysis along tubule. Fluorescence intensities of ER reporter (green) and protein (red) from line scans are presented as graphs. Scale bar, 0.5 μm. (B) Based on line scan analysis of peripheral ER tubules, percent localization of calnexin and derlin-1 puncta to ERmoxGFP or Sec61βGFP maxima and minima was quantified. Values plotted are mean ± SEM from three independent experiments (40 tubules per repeat) with one-way ANOVA for significance. \*\*\**P* < 0.001. Numerical values that underlie the graphs are shown in *S1 Data*. (C) Based on line scan analysis of peripheral ER tubules, percent localization of calnexin and derlin-1 puncta to ERmoxGFP maxima and minima was quantified in cells transfected with siCTL, siCLIMP-63, or siRTN4. Significance was assessed by  $\chi^2$  test from three independent experiments (20–40 tubules per repeat). \*\*\**P* < 0.001. Numerical values that underlie the graphs are shown in *S1 Data*. (D) Based on line scan analysis of peripheral ER tubules, percent localization of calnexin puncta to ERmoxGFP maxima and minima was quantified in HT-1080 cells cotransfected with mCherry-CLIMP-63, mCherry-RTN4a, or mCherry-ATL1 compared with CTL. Significance assessed by  $\chi^2$  test from three independent experiments (40 tubules per repeat). \*\*\**P* < 0.001. Numerical values that underlie the graphs are shown in *S1 Data*. ATL, atlastin; CLIMP-63, cytoskeleton-linking membrane protein 63; CTL, control; ER, endoplasmic reticulum; ERmoxGFP, ER monomeric oxidizing environment-optimized green fluorescent protein; ns, not significant; RTN4a, reticulon4a; siCLIMP-63, siRNA to CLIMP-63; siCTL, siControl; siRTN4, siRNA to RTN4.

<https://doi.org/10.1371/journal.pbio.3000355.g005>

luminal domain length and organization and thereby impact overlap of luminal and protein-enriched nanodomains along ER tubules.

## RTN4a and CLIMP-63 regulate luminal nanodomain dynamics in peripheral ER tubules

To determine whether CLIMP-63 and RTN impact the dynamics of ERmoxGFP luminal nanodomains, we acquired high-speed (40 ms/frame) 2D STED time-lapse image series of small ROIs encompassing individual peripheral ER tubules (Fig 6A). Kymograms of 100 frames over 4 seconds show increased ERmoxGFP intensity in select locations along the tubule (Fig 6B). This accumulation is indicative of luminal filling of localized nanodomains that is reported as peaks when fluorescence intensity along the tubule is averaged over time (Fig 6C). The coefficient of variation (CoV) along the tubule length of the normalized average fluorescent intensity over time provides a means to quantify the extent to which the luminal ERmoxGFP reporter accumulates stably at defined locations along peripheral ER tubules (Fig 6D). mCherry-CLIMP-63 overexpression disrupts the localized distribution of luminal ER nanodomains, while mCherry-RTN4a overexpression enhances the stability of these domains (Fig 6A; S3 Video). Conversely, siRTN4 knockdown showed a similar effect to CLIMP-63 overexpression, such that local stable accumulation of the luminal reporter at discrete sites along ER tubules is no longer observed (Fig 6B; S3 Fig; S4 Video). CLIMP-63 knockdown did not affect luminal ER nanodomain stability (Fig 6B; S3 Fig; S4 Video). The latter is consistent with the absence of an effect of CLIMP-63 siRNA on ERmoxGFP maxima length (Fig 2C). Dynamic luminal ERmoxGFP distribution along peripheral ER tubules therefore occurs within the framework of stable nanodomains whose ability to preferentially accumulate the luminal ERmoxGFP reporter is regulated by RTN4a and CLIMP-63.

## Discussion

Peripheral ER tubules are heterogenous, periodic structures composed of discrete nanodomains. STED imaging of luminal (ERmoxGFP) or membrane (Sec61 $\beta$ GFP) ER reporters, of CRISPR/Cas9 knock-in calreticulin-GFP expressed at endogenous levels, and of various antibody-labeled ER-resident proteins shows that ER proteins are localized to discrete puncta interspersed with luminal domains along ER tubules. Periodic distribution of ER reporters along ER tubules can be observed in various publications studying ER using various super-resolution microscope approaches and EM [13,27–32] and has more recently been reported by live cell GI-SIM [19]. However, the nanodomain organization of ER tubules and the mechanisms that underlie it have yet to be characterized. We show here that the ER-shaping proteins RTN4a and CLIMP-63 regulate the size and stability of luminal ER nanodomains and their overlap with resident ER proteins.

Single particle tracking has identified active luminal flow within ER tubules [18]. By high-speed 2D STED imaging, ER luminal periodicities are highly dynamic and present rapid oscillations (Fig 1; S1, S3 and S4 Videos). We interpret ERmoxGFP periodicities to reflect regions or nanodomains along ER tubules that preferentially accumulate or are filled with this luminal ER reporter. Localized distribution of these luminal periodicities along ER tubules over time suggests that these sites (blobs/maxima) are propitious to accumulation of the luminal reporter, relative to adjacent minima that limit luminal reporter accumulation. RTN4 knockdown or CLIMP-63 overexpression reduces, while RTN4a overexpression enhances the stability of sites of luminal reporter accumulation along ER tubules. These data suggest that these two ER-shaping proteins regulate luminal domain spacing along peripheral ER tubules. Our data do not, however, report directly on the diffusion of the luminal ERmoxGFP reporter in ER tubules. The relationship between RTN4a and CLIMP-63 regulation of ER nanodomains and the slower diffusion of luminal ER reporters in ER tubules relative to cytoplasm [33] or

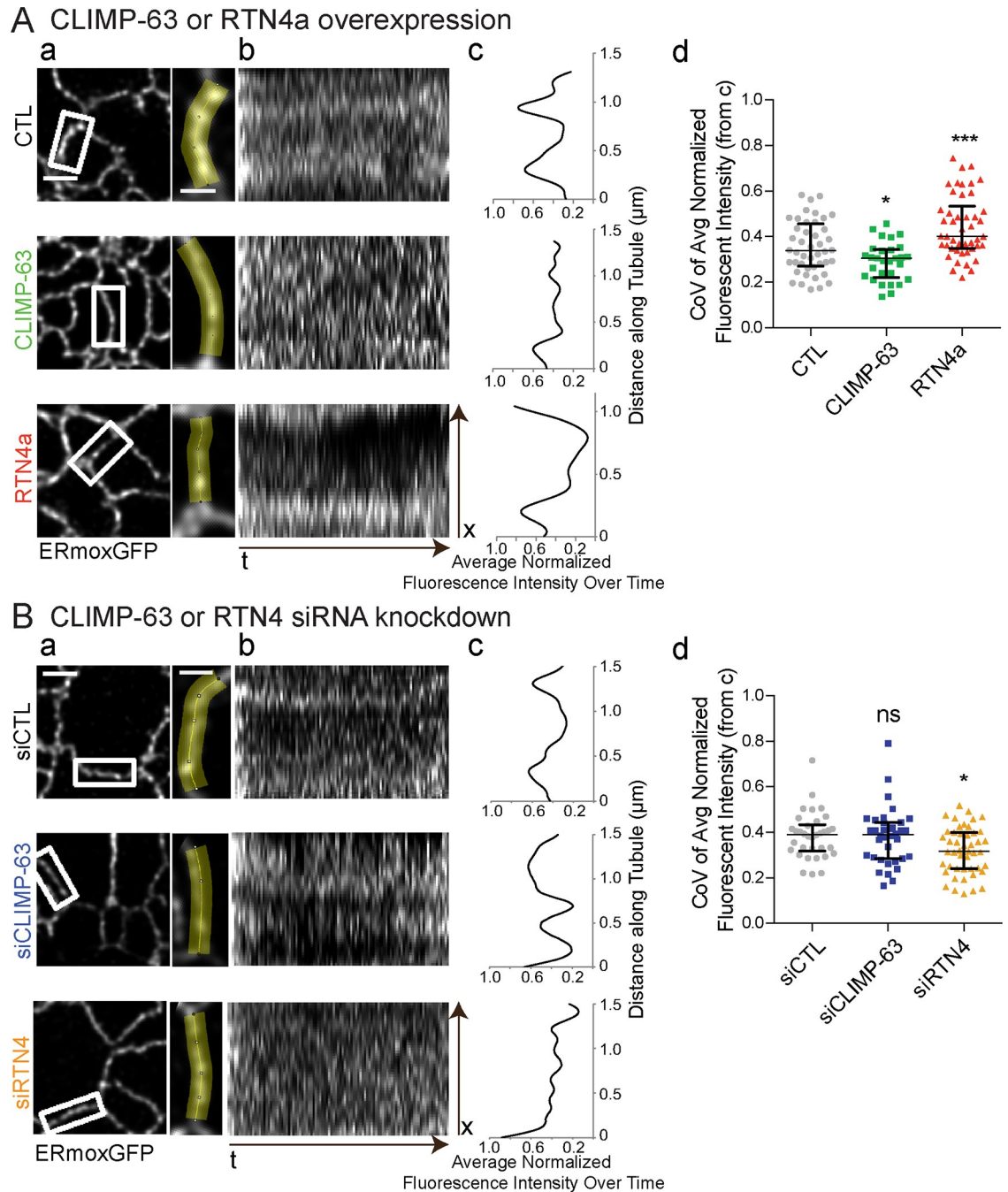


**Fig 6. RTN4a and CLIMP-63 regulate dynamics of luminal nanodomain compartmentalization along peripheral ER tubules.** STED live cell imaging (40 ms/frame over 4 seconds) of isolated ROIs of peripheral ERmoxGFP-labeled tubules (a) was performed for COS-7 cells cotransfected with mCherry-CLIMP-63 or mCherry-RTN4a (A) or transfected with siCLIMP-63, siRTN4, or siCTL (B). Kymographs show the distribution of ERmoxGFP at specific sites along ER tubules over time (b). From plots of normalized average intensity over time (c), we determined the CoV along the tubule length as a measure of localized distribution of ERmoxGFP to distinct domains along peripheral ER tubules (d). Scatter dot plots show median with interquartile range from three independent experiments (20–50 tubules per condition) with one-way ANOVA for significance. \*  $P < 0.05$ ; \*\*\*  $P < 0.001$ . Numerical values that underlie the plots are shown in [S1 Data](#). CLIMP-63, cytoskeleton-linking membrane protein 63; CoV, coefficient of variation; CTL, control; ER, endoplasmic reticulum; ERmoxGFP, ER monomeric oxidizing environment-optimized green fluorescent protein; ns, not significant; ROI, region of interest; RTN4a, reticulon4a; siCLIMP-63, siRNA to CLIMP-63; siCTL, siControl; siRNA, small interfering RNA; siRTN4, siRNA to RTN4; STED, stimulated emission depletion.

<https://doi.org/10.1371/journal.pbio.3000355.g006>

the contractions associated with nano-peristalsis along ER tubules [18] remains to be determined.

The RTNs cause local ER curvature [9], and CLIMP-63 maintains ER architecture by forming coiled-coil structures that maintain luminal spacing [6,34]. Knockdown of CLIMP-63 has been reported to decrease the width of ER sheets from 45.5 nm to 27.9 nm [6]. Although CLIMP-63 is predominantly associated with ER sheets [6,34], it is also expressed in peripheral ER tubules [13]. Paralleling the macro level segregation of these two ER-shaping proteins [6], RTN4a segregates away from and CLIMP-63 associates with luminal ERmoxGFP nanodomains. Alternating RTN4a membrane constriction and CLIMP-63 spacer functions along ER tubules could explain the luminal ER periodicity that we report here. Indeed, a recent study of luminal mEmerald-KDEL dynamics in peripheral ER tubules attributed the periodic distribution of this reporter to constrictions and bulges along the tubule length [19], as observed by EM [13,35–37]. However, ER tubule width is below the 70–80 nm STED resolution obtained in this study, and our data cannot therefore report on changes in ER tubule width. Furthermore, the fact that ERmoxGFP minima overlap with ER protein densities (Fig 5A and 5B) argues that luminal minima are not necessarily constrictions of the ER membrane itself. Mechanisms that control luminal filling of peripheral ER nanodomains may be related not only to tubule width (i.e., constrictions versus bulges) but also to occlusion of luminal space within the tubules by ER-resident protein complexes.

Indeed, by STED imaging, puncta of various ER proteins (calnexin, derlin-1, Gp78, BiP, and Stx17) along ER tubules were closely associated with RTN-associated luminal ERmoxGFP minima and therefore segregated away from luminal nanodomains. Overexpression or knockdown of either CLIMP-63 or RTN4a disrupted the enrichment of resident ER proteins in nanodomains depleted of the luminal ERmoxGFP reporter. Simplistically, increased ER tubule luminal filling due to CLIMP-63 overexpression or RTN4 knockdown could facilitate overlap between resident ER proteins and fluid components, while, conversely, localized accumulation of overexpressed RTN along ER tubules may sequester both protein and luminal ER tubule components away from RTN-enriched nanodomains. The fact that CLIMP-63 knockdown had minimal effect on luminal nanodomain stability and distribution argues that it is but one of multiple redundant mechanisms to define luminal enriched ER nanodomains. Regulation of ER nanodomain organization by these ER-shaping proteins in peripheral ER tubules parallels their roles in the formation of ER tubules and ER sheets. RTN and CLIMP-63 also contribute to nanohole formation in ER sheets [17], and together, these studies suggest that ER-shaping proteins play critical roles in the determination of ER morphology from the macro- to the nanoscale.

This study suggests that ER tubules are composed of protein-enriched nanodomains interspersed with fluid-filled nanodomains that may facilitate diffusion and exchange of small molecules, such as metabolites and enzyme substrates, as well as folding intermediates between protein complexes. The minimal overlap between the two endogenous ER markers studied, calnexin and derlin-1, suggests that multiple, discrete protein complexes exist within the ER. Further study is required to define how nanodomain organization and heterogeneity within the highly dynamic ER tubular network control functional interaction between ER-resident proteins, cargo proteins, enzymatic substrates, and metabolites to enable ER quality control and cargo processing.

## Materials and methods

### Plasmids, antibodies, and chemicals

ERmoxGFP was a gift from Dr. Erik Snapp (Albert Einstein College of Medicine, presently at Howard Hughes Medical Institute Janelia Research Campus, VA) (Addgene plasmid #68072),

mCherry-CLIMP-63 and Sec61 $\beta$ GFP from Dr. Gia Voeltz (University of Colorado, Boulder, CO), Sec61 $\beta$ mRFP from Dr. Patrick Lajoie (University of Western Ontario, London, ON, Canada), and mCherry-RTN4a and mCherry-ATL1 from Dr. Tom Rapoport (Harvard University, MA) (Addgene plasmid #86683 and #86678, respectively). Anti-CLIMP-63 antibody (G1/296) was purchased from Enzo Life Sciences (Farmingdale, NY) (Cat# ALX-804-604-C100). Rabbit anti-calnexin (Cat# C4731), mouse anti-derlin-1 (Cat# SAB4200148), rabbit anti-BiP (Cat# G9043), mouse anti-actin (Cat# A2228), goat anti-mouse HRP conjugate (Cat# AP308P), goat anti-rabbit HRP conjugate (Cat# AP307P), and rabbit anti-Stx17 (Cat# HPA001204) antibodies were from Sigma (St. Louis, MO). Rabbit anti-RTN4/NOGO (Cat# 10950-1-AP) and anti-Gp78 (Cat# 16675-1-AP) antibodies were from Proteintech (Rosemont, IL). Goat serum (Cat# 16210-064), goat anti-rabbit IgG (H+L) cross-adsorbed secondary antibody, Alexa Fluor 532 (Cat# A-11009), and goat anti-mouse IgG (H+L) cross-adsorbed secondary antibody, Alexa Fluor 568 (Cat# A-11004) were from Thermo Fisher Scientific (Waltham, MA). siCLIMP-63 (Cat# L-012755-01-0005), siRTN4 (L-010721-00-0005) and nontargeting Control siRNA (Cat# D-001810-01-50) were from Dharmacon, GE Healthcare Life Sciences (Chicago, IL). Sixteen percent paraformaldehyde (Cat# 15710) and 25% glutaraldehyde (Cat# 16220) were from Electron Microscopy Sciences (Hatfield, PA), USA. Other chemicals were from Sigma (St. Louis, MO).

### Cell culture, transfection, and western blot

HT-1080 cells were grown at 37°C with 5% CO<sub>2</sub> in complete RPMI 1640 (Thermo Fisher Scientific, Waltham, MA) containing 10% fetal bovine serum (FBS) (Thermo Fisher Scientific, Waltham, MA) and 1% L-glutamine (Thermo Fisher Scientific, Waltham, MA) unless otherwise stated. The U2OS knock-in cell line expressing GFP-calreticulin at endogenous levels generated with CRISPR/Cas technology was provided by Dr. Tom Rapoport (Harvard University, MA). COS-7 and U2OS cells were grown at 37°C with 5% CO<sub>2</sub> in complete DMEM (Thermo Fisher Scientific, Waltham, MA) containing 10% FBS and 1% L-glutamine. All cell lines were mycoplasma-free, tested routinely by PCR (Applied Biological Materials, Richmond, BC, Canada) and, as necessary, treated with BM Cyclin (Roche, Mannheim, Germany) to eliminate mycoplasma contamination.

Plasmids were transfected for 22 hours using Effectene (Qiagen, Hilden, Germany) according to the manufacturer's protocols. siRNA transfection was done with Lipofectamine 2000 Transfection Reagent (Thermo Fisher Scientific, Waltham, MA) in Opti-MEM Reduced Serum Media (Thermo Fisher Scientific, Waltham, MA), which was replaced with fresh complete RPMI 1640 after 5 hours; after a further 21 hours plasmids were transfected with Effectene and incubated for 22 hours before fixation. For live cell imaging, cells were grown in ibidi 8-well  $\mu$ -slides with #1.5H (170  $\mu$ m  $\pm$  5  $\mu$ m) D 263 M Schott glass and transfected as described above. For live cell imaging at 37°C, complete RPMI 1640 medium was replaced with warmed RPMI 1640 medium (Sigma, St. Louis, MO) without sodium bicarbonate, supplemented with 1% L-glutamine, 10% FBS, 10% HEPES (Thermo Fisher Scientific, Waltham, MA) for HT-1080 cells. For COS-7 and U2OS cells, complete DMEM medium was replaced by FluoroBrite DMEM media (Thermo Fisher Scientific, Waltham, MA) warmed to 37°C before imaging. Western blots were conducted as previously described [38].

### Immunofluorescence labeling

Cells grown on #1.5H coverslips (Paul Marienfeld, Lauda-Königshofen, Germany) were (1) fixed with 3% paraformaldehyde with 0.2% glutaraldehyde in phosphate-buffered saline (PBS) at room temperature for 15 minutes and washed with PBS-CM (PBS supplemented with 0.1

mM CaCl<sub>2</sub> and 1 mM MgCl<sub>2</sub>; two quick washes and then two 5-minute washes); (2) permeabilized with 0.2% Triton X-100 for 5 minutes, then washed with PBS-CM as above; (3) quenched with 1 mg/mL of NaBH<sub>4</sub> (Sigma, USA) for 10 minutes and washed with PBS-CM; (4) blocked with 10% Goat Serum (Thermo Fisher Scientific, Waltham, MA) and 1% bovine serum albumin (Sigma, St. Louis, MO) in PBS-CM for 1 hour; (5) incubated with primary antibodies in Antibody Buffer (1% BSA, 2% goat serum, 0.05% Triton-X100 in saline-sodium citrate buffer in Milli-Q H<sub>2</sub>O) overnight at 4°C, then washed with PBS-CM, then three times for 5 minutes with Antibody Wash Buffer (saline-sodium citrate buffer, 0.05% Triton-X100 in Milli-Q H<sub>2</sub>O); (6) incubated with secondary antibodies in Antibody Buffer for 1 hour, then washed with PBS-CM, then six times for 10 minutes with Antibody Wash Buffer on a rocker; and (7) rinsed with Milli-Q H<sub>2</sub>O and mounted with ProLong Diamond (Thermo Fisher Scientific, Waltham, MA) and cured for 24–48 hours at room temperature.

### Confocal and STED microscopy

Confocal and STED imaging was performed with the 100×/1.4 Oil HC PL APO CS2 STED White objective of a Leica TCS SP8 3× STED microscope (Leica, Wetzlar, Germany) equipped with a white light laser, HyD detectors, and Leica Application Suite X (LAS X) software (LSI IMAGING, Life Sciences Institute, University of British Columbia). Time-gated fluorescence detection was used for STED to further improve lateral resolution. Live cell time-lapse imaging of GFP-tagged reporters was performed at 37°C using the 592-nm depletion laser on a 15,360-nm square ROI (0.8-second frame rate over 40 seconds) or a 3,840-nm square ROI (40-ms frame rate over 4 seconds) in the periphery of the cell. For double- or triple-labeled fixed samples, acquisition was done at a scan speed of 600 Hz with a line average of 6. GFP was excited at 488 nm and depleted using the 592-nm depletion laser. Alexa Fluor 532 was excited at 528 nm, Alex Fluor 568 at 577 nm, and mRFP at 584 nm, and all three were depleted using the 660-nm depletion laser. Sequential acquisition (in the order of AF568/AF532/GFP or mRFP/GFP) between frames (2D) or between stacks (3D) was used to avoid cross talk. Three-dimensional STED images were acquired at a step size of 100 nm. STED images were deconvolved using Huygens Professional software (Scientific Volume Imaging, Hilversum, the Netherlands) that was also used to determine the theoretical PSFs from 2D STED live and fixed images and from 3D STED fixed images. XY FWHM values obtained from the theoretical PSFs for STED GFP images were 70 nm for 2D fixed and 78 nm for 2D live. For 3D fixed analysis, FWHM was 126 nm for XY and 340 nm for Z.

### Quantification and statistical analysis

Line scan analysis of at least 40 peripheral ER tubules per sample was done using Leica LAS-X software. Spatially isolated peripheral tubules were selected for analysis based on the presence of a minimum of two protein puncta per tubule in the protein-labeled channel. A histogram of normalized fluorescence intensity (scale of 0–1) along the line was exported for the ER reporters (ERmoxGFP or Sec61βGFP) and either calnexin, derlin-1, mCherry-CLIMP-63, mCherry-RTN4a, or mCherry-ATL1, and displayed using GraphPad Prism (GraphPad Software, San Diego, CA). Maximum and minimum fluorescence values were identified with a Java script. Blobs were defined as local maxima in the fluorescence signal and minima as troughs in fluorescence intensity, at least 20% below both adjacent maxima. FWHM of maxima was used to determine blob length. The percent decrease in the fluorescence signal of all minima was calculated relative to the adjacent maximum of lower fluorescence. Protein (calnexin and derlin-1) puncta were localized to either maxima or minima and deemed intermediate if the puncta center was greater than 20 nm from the peak of the maxima or minima. Quantification of

protein puncta distribution to maxima and minima in 3D projections was scored manually in LAS-X. Three-dimensional STED volume rendering was done with LAS-X. Analysis of the live cell imaging (40 ms/frame) was done with ImageJ/FIJI [39]. General image processing (2D image exporting to tiff format and 3D volume rendering) and final image preparation (merging, zoom, cropping, and addition of the scale bar) for publication were performed using LAS-X and FIJI. Statistical analyses were done using Prism 6.0.

## Supporting information

**S1 Fig. Calnexin exhibits a punctate distribution along peripheral ER tubules independent of ERmoxGFP transfection.** Representative confocal and STED images of calnexin and ERmoxGFP in ERmoxGFP transfected and untransfected cells. The punctate distribution of calnexin is observed more readily by STED (raw and decon) compared with confocal imaging in both (A) transfected and (B) untransfected cells. Scale bar, 5  $\mu\text{m}$ ; zooms, 2  $\mu\text{m}$ . decon, deconvolution; ER, endoplasmic reticulum; ERmoxGFP, ER monomeric oxidizing environment-optimized green fluorescent protein; STED, stimulated emission depletion. (TIF)

**S2 Fig. ER-resident proteins are distributed to luminal minima of peripheral ER tubules.** (A) Quantification of 3D localization of calnexin and derlin-1 puncta to ERmoxGFP maxima and minima of peripheral ER tubules in 3D STED images of siCTL or siCLIMP-63 HT-1080 cells. Significance assessed by  $\chi^2$  test from at least 25 ROIs (2.5  $\mu\text{m} \times 2.5 \mu\text{m}$ ) from 10 three-dimensional stacks for each condition at 2 degrees of freedom in three independent experiments. \* $P < 0.05$ ; \*\* $P < 0.01$ . Numerical values that underlie the graphs are shown in [S1 Data](#). (B) Based on line scan analysis of peripheral ER tubules imaged by 2D STED, localization of BiP, Gp78, and Stx17 puncta to ERmoxGFP maxima and minima was quantified. Significance assessed by one-way ANOVA from at least 20 line scans in three independent experiments. \* $P < 0.05$ ; \*\* $P < 0.01$ ; \*\*\* $P < 0.001$ . Numerical values that underlie the graphs are shown in [S1 Data](#). BiP, binding immunoglobulin protein; ER, endoplasmic reticulum; ERmoxGFP, ER monomeric oxidizing environment-optimized green fluorescent protein; Gp78, glycoprotein 78; ROI, region of interest; siCTL, siControl; siCLIMP-63, siRNA to CLIMP-63; STED, stimulated emission depletion; Stx17, Syntaxin-17; 2D, two-dimensional; 3D, three-dimensional. (TIF)

**S3 Fig. RTN4 and CLIMP-63 and knockdown by siRNA in COS-7 cells.** Western blots of RTN4 and CLIMP-63 siRNA knockdown in COS-7 cells. The blots were probed with anti-CLIMP-63, anti-RTN4, or anti- $\beta$ -actin as a loading control. CLIMP-63, cytoskeleton-linking membrane protein 63; RTN4, reticulon4; siRNA, small interfering RNA. (TIF)

**S1 Video. Live cell STED imaging reveals ER periodicity.** Live HT-1080 cells overexpressing ERmoxGFP or Sec61 $\beta$ GFP were imaged with confocal or STED at 37°C for 40 seconds at a temporal resolution of 0.8 seconds per frame. (a) Confocal ERmoxGFP; (b) STED ERmoxGFP; (c) confocal Sec61 $\beta$ GFP; (d) STED Sec61 $\beta$ GFP. Video frame rate: 10 frames per second. ER, endoplasmic reticulum; ERmoxGFP, ER monomeric oxidizing environment-optimized green fluorescent protein; STED, stimulated emission depletion. (MP4)

**S2 Video. Three-channel 3D STED imaging of calnexin and derlin-1 puncta localized to ER tubule minima.** ERmoxGFP expressing HT-1080 cells were fixed, labeled with calnexin and derlin-1, and imaged sequentially (derlin-1, calnexin, and ERmoxGFP) with 3D STED

(vortex donut enabled). Video frame rate: 10 frames per second. ER, endoplasmic reticulum; ERmoxGFP, ER monomeric oxidizing environment-optimized green fluorescent protein; STED, stimulated emission depletion; 3D, three-dimensional.

(MP4)

**S3 Video. High-speed STED imaging of lumenal ER nanodomains upon RTN4a and CLIMP-63 overexpression.** Live COS-7 cells were transfected with ERmoxGFP (CTL) or cotransfected with ERmoxGFP and either mCherry-CLIMP-63 (CLIMP-63 OX) or mCherry-RTN4a (RTN OX). ERmoxGFP was imaged with STED at 37°C over 4 seconds at a temporal resolution of 40 ms per frame. Arrows show sites of stable distribution of ERmoxGFP at specific sites along ER tubules over time, as determined by kymogram analysis (Fig 6). Video frame rate: 10 frames per second. CLIMP-63, cytoskeleton-linking membrane protein 63; CTL, control; ER, endoplasmic reticulum; ERmoxGFP, ER monomeric oxidizing environment-optimized green fluorescent protein; OX, over-expression; RTN4a, reticulon4a; STED, stimulated emission depletion.

(MP4)

**S4 Video. High-speed STED imaging of lumenal ER nanodomains upon RTN4 and CLIMP-63 knockdown.** Live COS-7 cells were transfected with siCTL, siCLIMP-63, or siRTN4, as indicated, and then with ERmoxGFP. ERmoxGFP was imaged with STED at 37°C over 4 seconds at a temporal resolution of 40 ms per frame. Arrows show sites of stable distribution of ERmoxGFP at specific sites along ER tubules over time, as determined by kymogram analysis (Fig 6). Video frame rate: 10 frames per second. CLIMP-63, cytoskeleton-linking membrane protein 63; ER, endoplasmic reticulum; ERmoxGFP, ER monomeric oxidizing environment-optimized green fluorescent protein; RTN4, reticulon4; siCLIMP-63, siRNA to CLIMP-63; siCTL, siControl; siRTN4, siRNA to RTN4; STED, stimulated emission depletion.

(MP4)

**S1 Data. Numerical values associated with graphs and plots in figures and supporting information.**

(XLSX)

## Acknowledgments

We thank Dr. Christopher Loewen (UBC) for helpful discussions. Imaging was performed at the UBC Life Sciences Institute Imaging Core Facility (*LSI IMAGING*).

## Author Contributions

**Conceptualization:** Guang Gao, Ivan R. Nabi.

**Data curation:** Guang Gao, Chengjia Zhu, Emma Liu.

**Formal analysis:** Guang Gao, Chengjia Zhu, Emma Liu, Ivan R. Nabi.

**Funding acquisition:** Ivan R. Nabi.

**Investigation:** Guang Gao, Chengjia Zhu, Emma Liu.

**Methodology:** Guang Gao, Chengjia Zhu, Emma Liu, Ivan R. Nabi.

**Project administration:** Ivan R. Nabi.

**Resources:** Ivan R. Nabi.

**Software:** Guang Gao.

**Supervision:** Guang Gao, Ivan R. Nabi.

**Validation:** Guang Gao.

**Visualization:** Guang Gao.

**Writing – original draft:** Guang Gao, Ivan R. Nabi.

**Writing – review & editing:** Guang Gao, Ivan R. Nabi.

## References

1. Kusumi A, Fujiwara TK, Chadda R, Xie M, Tsunoyama TA, Kalay Z, et al. Dynamic organizing principles of the plasma membrane that regulate signal transduction: commemorating the fortieth anniversary of Singer and Nicolson's fluid-mosaic model. *Ann Rev Cell Dev Biol.* 2012; 28:215–50.
2. Shibata Y, Voeltz GK, Rapoport TA. Rough sheets and smooth tubules. *Cell.* 2006; 126(3):435–9. <https://doi.org/10.1016/j.cell.2006.07.019> PMID: 16901774
3. Voeltz GK, Prinz WA, Shibata Y, Rist JM, Rapoport TA. A class of membrane proteins shaping the tubular endoplasmic reticulum. *Cell.* 2006; 124(3):573–86. <https://doi.org/10.1016/j.cell.2005.11.047> PMID: 16469703
4. Hu J, Shibata Y, Zhu PP, Voss C, Rismanchi N, Prinz WA, et al. A class of dynamin-like GTPases involved in the generation of the tubular ER network. *Cell.* 2009; 138(3):549–61. <https://doi.org/10.1016/j.cell.2009.05.025> PMID: 19665976
5. Westrate LM, Lee JE, Prinz WA, Voeltz GK. Form follows function: the importance of endoplasmic reticulum shape. *Ann Rev Biochem.* 2015; 84:791–811. <https://doi.org/10.1146/annurev-biochem-072711-163501> PMID: 25580528
6. Shibata Y, Shemesh T, Prinz WA, Palazzo AF, Kozlov MM, Rapoport TA. Mechanisms determining the morphology of the peripheral ER. *Cell.* 2010; 143(5):774–88. <https://doi.org/10.1016/j.cell.2010.11.007> PMID: 21111237
7. Anwar K, Klemm RW, Condon A, Severin KN, Zhang M, Ghirlando R, et al. The dynamin-like GTPase Sey1p mediates homotypic ER fusion in *S. cerevisiae*. *J Cell Biol.* 2012; 197(2):209–17. <https://doi.org/10.1083/jcb.201111115> PMID: 22508509
8. Orso G, Pendin D, Liu S, Tosetto J, Moss TJ, Faust JE, et al. Homotypic fusion of ER membranes requires the dynamin-like GTPase atlastin. *Nature.* 2009; 460(7258):978–83. <https://doi.org/10.1038/nature08280> PMID: 19633650
9. Zhang H, Hu J. Shaping the Endoplasmic Reticulum into a Social Network. *Trends Cell Biol.* 2016; 26(12):934–43. <https://doi.org/10.1016/j.tcb.2016.06.002> PMID: 27339937
10. Shibata Y, Voss C, Rist JM, Hu J, Rapoport TA, Prinz WA, et al. The reticulon and DP1/Yop1p proteins form immobile oligomers in the tubular endoplasmic reticulum. *J Biol Chem.* 2008; 283(27):18892–904. <https://doi.org/10.1074/jbc.M800986200> PMID: 18442980
11. Hu J, Shibata Y, Voss C, Shemesh T, Li Z, Coughlin M, et al. Membrane proteins of the endoplasmic reticulum induce high-curvature tubules. *Science.* 2008; 319(5867):1247–50. <https://doi.org/10.1126/science.1153634> PMID: 18309084
12. Lewis SC, Uchiyama LF, Nunnari J. ER-mitochondria contacts couple mtDNA synthesis with mitochondrial division in human cells. *Science.* 2016; 353(6296):aaf5549. <https://doi.org/10.1126/science.aaf5549> PMID: 27418514
13. Nixon-Abell J, Obara CJ, Weigel AV, Li D, Legant WR, Xu CS, et al. Increased spatiotemporal resolution reveals highly dynamic dense tubular matrices in the peripheral ER. *Science.* 2016; 354(6311).
14. Bernales S, McDonald KL, Walter P. Autophagy counterbalances endoplasmic reticulum expansion during the unfolded protein response. *PLoS Biol.* 2006; 4(12):e423. <https://doi.org/10.1371/journal.pbio.0040423> PMID: 17132049
15. Hell SW, Wichmann J. Breaking the diffraction resolution limit by stimulated emission: stimulated-emission-depletion fluorescence microscopy. *Optics Letters.* 1994; 19(11):780–2. <https://doi.org/10.1364/ol.19.000780> PMID: 19844443
16. Hein B, Willig KI, Hell SW. Stimulated emission depletion (STED) nanoscopy of a fluorescent protein-labeled organelle inside a living cell. *PNAS USA.* 2008; 105(38):14271–6. <https://doi.org/10.1073/pnas.0807705105> PMID: 18796604
17. Schroeder LK, Barentine AES, Merta H, Schweighofer S, Zhang Y, Baddeley D, et al. Dynamic nanoscale morphology of the ER surveyed by STED microscopy. *J Cell Biol.* 2019; 218(1):83–96. <https://doi.org/10.1083/jcb.201809107> PMID: 30442642

18. Holcman D, Parutto P, Chambers JE, Fantham M, Young LJ, Marciniak SJ, et al. Single particle trajectories reveal active endoplasmic reticulum luminal flow. *Nature Cell Biol.* 2018; 20(10):1118–25. <https://doi.org/10.1038/s41556-018-0192-2> PMID: 30224760
19. Guo Y, Li D, Zhang S, Yang Y, Liu JJ, Wang X, et al. Visualizing Intracellular Organelle and Cytoskeletal Interactions at Nanoscale Resolution on Millisecond Timescales. *Cell.* 2018; 175(5):1430–42 e17. <https://doi.org/10.1016/j.cell.2018.09.057> PMID: 30454650
20. Costantini LM, Baloban M, Markwardt ML, Rizzo M, Guo F, Verkhusha VV, et al. A palette of fluorescent proteins optimized for diverse cellular environments. *Nature Comm.* 2015; 6:7670.
21. Lewis MJ, Pelham HR. Ligand-induced redistribution of a human KDEL receptor from the Golgi complex to the endoplasmic reticulum. *Cell.* 1992; 68(2):353–64. [https://doi.org/10.1016/0092-8674\(92\)90476-s](https://doi.org/10.1016/0092-8674(92)90476-s) PMID: 1310258
22. Wang S, Tukachinsky H, Romano FB, Rapoport TA. Cooperation of the ER-shaping proteins atlastin, lunapark, and reticulons to generate a tubular membrane network. *eLife.* 2016; 5.
23. Loewen CJ, Roy A, Levine TP. A conserved ER targeting motif in three families of lipid binding proteins and in Opi1p binds VAP. *EMBO J.* 2003; 22(9):2025–35. <https://doi.org/10.1093/emboj/cdg201> PMID: 12727870
24. Moss TJ, Andrezza C, Verma A, Daga A, McNew JA. Membrane fusion by the GTPase atlastin requires a conserved C-terminal cytoplasmic tail and dimerization through the middle domain. *PNAS USA.* 2011; 108(27):11133–8. <https://doi.org/10.1073/pnas.1105056108> PMID: 21690399
25. Ye Y, Shibata Y, Yun C, Ron D, Rapoport TA. A membrane protein complex mediates retro-translocation from the ER lumen into the cytosol. *Nature.* 2004; 429(6994):841–7. <https://doi.org/10.1038/nature02656> PMID: 15215856
26. Chen W, Helenius J, Braakman I, Helenius A. Cotranslational folding and calnexin binding during glycoprotein synthesis. *PNAS USA.* 1995; 92(14):6229–33. <https://doi.org/10.1073/pnas.92.14.6229> PMID: 7541532
27. Caldieri G, Barbieri E, Nappo G, Raimondi A, Bonora M, Conte A, et al. Reticulon 3-dependent ER-PM contact sites control EGFR nonclathrin endocytosis. *Science.* 2017; 356(6338):617–24. <https://doi.org/10.1126/science.aah6152> PMID: 28495747
28. York AG, Chandris P, Nogare DD, Head J, Wawrzusin P, Fischer RS, et al. Instant super-resolution imaging in live cells and embryos via analog image processing. *Nature Methods.* 2013; 10(11):1122–6. <https://doi.org/10.1038/nmeth.2687> PMID: 24097271
29. Shim SH, Xia C, Zhong G, Babcock HP, Vaughan JC, Huang B, et al. Super-resolution fluorescence imaging of organelles in live cells with photoswitchable membrane probes. *PNAS USA.* 2012; 109(35):13978–83. <https://doi.org/10.1073/pnas.1201882109> PMID: 22891300
30. Takakura H, Zhang Y, Erdmann RS, Thompson AD, Lin Y, McNellis B, et al. Long time-lapse nanoscopy with spontaneously blinking membrane probes. *Nature Biotech.* 2017.
31. Bottanelli F, Kromann EB, Allgeyer ES, Erdmann RS, Wood Baguley S, Sirinakis G, et al. Two-colour live-cell nanoscale imaging of intracellular targets. *Nature Comm.* 2016; 7:10778.
32. Huang F, Sirinakis G, Allgeyer ES, Schroeder LK, Duim WC, Kromann EB, et al. Ultra-High Resolution 3D Imaging of Whole Cells. *Cell.* 2016; 166(4):1028–40. <https://doi.org/10.1016/j.cell.2016.06.016> PMID: 27397506
33. Dayel MJ, Hom EF, Verkman AS. Diffusion of green fluorescent protein in the aqueous-phase lumen of endoplasmic reticulum. *Biophys J.* 1999; 76(5):2843–51. [https://doi.org/10.1016/S0006-3495\(99\)77438-2](https://doi.org/10.1016/S0006-3495(99)77438-2) PMID: 10233100
34. Klopfenstein DR, Klumperman J, Lustig A, Kammerer RA, Oorschot V, Hauri HP. Subdomain-specific localization of CLIMP-63 (p63) in the endoplasmic reticulum is mediated by its luminal alpha-helical segment. *J Cell Biol.* 2001; 153(6):1287–300. <https://doi.org/10.1083/jcb.153.6.1287> PMID: 11402071
35. Behnke O, Moe H. An Electron Microscope Study of Mature and Differentiating Paneth Cells in the Rat, Especially of Their Endoplasmic Reticulum and Lysosomes. *J Cell Biol.* 1964; 22:633–52. <https://doi.org/10.1083/jcb.22.3.633> PMID: 14206428
36. West M, Zurek N, Hoenger A, Voeltz GK. A 3D analysis of yeast ER structure reveals how ER domains are organized by membrane curvature. *J Cell Biol.* 2011; 193(2):333–46. <https://doi.org/10.1083/jcb.201011039> PMID: 21502358
37. Friedman JR, Voeltz GK. The ER in 3D: a multifunctional dynamic membrane network. *Trends Cell Biol.* 2011; 21(12):709–17. <https://doi.org/10.1016/j.tcb.2011.07.004> PMID: 21900009
38. Meng F, Saxena S, Liu Y, Joshi B, Wong TH, Shankar J, et al. The phospho-caveolin-1 scaffolding domain dampens force fluctuations in focal adhesions and promotes cancer cell migration. *Mol Biol Cell.* 2017; 28(16):2190–201. <https://doi.org/10.1091/mbc.E17-05-0278> PMID: 28592633

39. Schindelin J, Arganda-Carreras I, Frise E, Kaynig V, Longair M, Pietzsch T, et al. Fiji: an open-source platform for biological-image analysis. *Nature Methods*. 2012; 9(7):676–82. <https://doi.org/10.1038/nmeth.2019> PMID: [22743772](https://pubmed.ncbi.nlm.nih.gov/22743772/)